Temperature dependence of capillary dynamics: A multiphase and multicomponent adiabatic approach

Federico Maggi* and Fernando Alonso-Marroquin
School of Civil Engineering, University of Sydney, Sydney 2006, NSW, Australia
(Received 27 August 2013; revised manuscript received 22 October 2013; published 15 November 2013)

We present an analysis of the effect of the temperature on the flow of multiphase systems made of multiple miscible components in uniform cylindrical capillaries in adiabatic conditions. The temperature was explicitly included in the dynamic contact angle, tension at the three-phase contact line, and densities and viscosities of the fluids. The mathematical framework accounted for conservative forces (gravity, inertial, and interfacial tensions), nonconservative forces (viscous dissipation), and fluid retardation effects in the reservoirs at the two capillary ends. Temperature-dependent flow regimes ranged from nonoscillatory to oscillatory in a two-phase binary liquid (water-ethanol) system and in a two-phase pure liquid (ether) system. The Ca-Bo orbits highlighted dynamic attractors that depended on specific system characteristics as well as temperature. We conclude that temperature alone expresses and important role in the dynamical characteristics of capillary rise flow around its equilibrium.

DOI: 10.1103/PhysRevE.88.053013 PACS number(s): 47.55.nb

I. INTRODUCTION

The physical description of capillary flows initiated by Bell and Cameron [1] and followed by Lucas [2] and Washburn [3] set the mathematical basis of what is known as the Lucas-Washburn (LW) equation. For single-phase systems (typically liquids), the LW equation has been developed to a remarkably high accuracy after Blake and Haynes [4], Szekely *et al*. [5], Levine *et al*. [6], and Dreyer *et al*. [7] among others. However, only recently has the attention focused on the dynamics of multiphase (gas-liquid) capillary rise (e.g., Refs. [8–10]), while less work has been devoted on the inclusion of multicomponent systems such as liquid or gaseous mixtures [11]. There is an additional aspect of the dynamics of capillary rise that deserve to be investigated to a greater detail: when chemical and physical properties at different temperatures affect the overall dynamics. Temperature substantially affects the surface tension at the gas-liquid and liquid-liquid interfaces [12], the mass exchange between the gas and liquid phases (e.g., evaporation) [13], the density and viscosity of the fluids, and the contact angle [14,15]. In instances where these quantities scale nonlinearly with the temperature, a nontrivial balance between conservative and nonconservative forces may result at different temperatures. An example of multiphase capillary flow that is particularly susceptible to the temperature is the capillary rise of ether (and light liquids in general) when the meniscus is approaching the equilibrium height. At room temperature, this system typically shows oscillatory dynamics in capillaries with suitable radius [8,16,17], while a lower temperature can change these dynamics to nonoscillatory. A further example is when miscible liquids are used, which may show high composition-dependent nonlinearities in density, viscosity, and surface tension that add a degree of complexity to capillary flows at different temperatures.

Whereas explanations of oscillatory to nonoscillatory transitions in single-phase capillary flows have been largely devoted to the interplay between capillary radius, liquid viscosity, and gravitational acceleration (e.g., Refs. [8,16–19]), the overall effect of temperature in determining these transitions under adiabatic or nonadiabatic conditions has not been clarified yet in either multiphase single-component systems or multiphase multicomponent systems.

The aim of this work is to explicitly include the temperature in a mechanistic description of multiphase and multicomponent flows in capillaries. The focus here is on adiabatic systems, as nonadiabatic conditions can lead to phase changes and nonlinearities (e.g., Marangoni effect) that are beyond the purpose of this work. The mechanistic framework used here describes the transient meniscus velocity within a uniform cylindrical capillary under the action of conservative forces (gravity), nonconservative forces (viscous drag along the capillary, and energy dissipation at the meniscus), and the retardation effects of the fluids in the reservoirs at the two capillary ends. Temperature is taken into account in the description of dynamics contact angle, surface tension, density, and viscosity of both phases within the capillary, and for any generic mixture of multiple miscible components of the liquid phase. The framework presented here is used with experimental data of the rise of air-water-ethanol and air-ether in a glass capillary at various constant temperatures to elucidate the effect of temperature on these systems. It is anticipated here that these analyses show that temperature plays a major role in determining the overall steady state and transient state of capillary processes, and in the transition to the oscillatory regime.

II. METHODS

A. Liquid-gas capillary dynamics

The dynamics of multiphase fluids in uniform cylindrical capillaries of length L and radius R can be described by the simultaneous action of gravitational and viscous forces, tension at the gas-liquid interface, dissipative forces localized at the capillary outlet (jet flow), and the inertial effects of the fluid in the feeding reservoir at the capillary inlet. The resulting second-order nonlinear differential equation of the meniscus

*federico.maggi@sydney.edu.au

acceleration can be expressed as [9]

$$\left[1+\frac{7}{6}\frac{\rho_l}{L\rho(h)}R\right]h''=\frac{2\gamma\cos(\theta_\infty)}{RL\rho(h)}-\frac{2A\gamma\,\mathrm{arcsinh}(Bh')}{RL\rho(h)}-\frac{8\mu(h)}{R^2\rho(h)}h'-g\left[1-\frac{\rho_g}{\rho(h)}\right]-\frac{1}{2}\frac{\rho_l-\rho_g}{L\rho(h)}h'^2-\frac{1}{6}\frac{\rho_l}{L\rho(h)}h'^2 \quad \text{for} \quad h'\geqslant 0, \tag{1a}$$

$$\left[1+\frac{7}{6}\frac{\rho_g}{L\rho(h)}R\right]h''=\frac{2\gamma\cos(\theta_\infty)}{RL\rho(h)}-\frac{2A\gamma\,\mathrm{arcsinh}(Bh')}{RL\rho(h)}-\frac{8\mu(h)}{R^2\rho(h)}h'-g\left[1-\frac{\rho_g}{\rho(h)}\right]-\frac{1}{2}\frac{\rho_l-\rho_g}{L\rho(h)}h'^2+\frac{1}{6}\frac{\rho_g}{L\rho(h)}h'^2 \quad \text{for} \quad h'<0, \tag{1b}$$

where h, h', and h'' are the time-dependent meniscus position, velocity, and acceleration, respectively, and γ is the surface tension at the solid-liquid-gas contact line. The functions $\rho(h)$ and $\mu(h)$ are defined as

$$\rho(h)=[\rho_l h+\rho_g(L-h)]/L, \tag{2a}$$

$$\mu(h)=[\mu_l h+\mu_g(L-h)]/L \tag{2b}$$

and represent the average density and viscosity within the capillary, with subscripts l and g indicating the liquid and gaseous phases, respectively.

The dynamic contact angle was expressed in Eqs. (1) as a function of the contact angle at rest θ_∞ and the meniscus velocity as [4]

$$\cos(\theta)=\cos(\theta_\infty)-A\,\mathrm{arcsinh}\{Bh'\} \tag{3}$$

with A and B two functions of the molecular and thermodynamic interface properties expressed as

$$A=\frac{2nk_BT}{\gamma},\quad B=\frac{1}{2K^0\lambda}, \tag{4}$$

where n is the number of affected adsorption sites at the solid and liquid interfaces per unit area of solid interface, $k_B=1.38\times10^{-23}$ J/K is the Boltzmann constant, T the temperature in degrees Kelvin, $\lambda\approx n^{-1/2}$ the average distance between adsorption sites, and K^0 the rate constant describing the frequency of molecular displacements at the three-phase contact line [4,20].

In including the gaseous and liquid phases in the capillary flow of Eqs. (1), adiabatic conditions were assumed, and hence heat flow was not described explicitly and neither was energy balance included. These working hypotheses are suitable only for systems in thermal equilibrium, whereas they could fail in nonadiabatic conditions, where heat exchange through the boundaries, latent heat, as well as temperature gradients could cause changes in phases or could produce surface tension gradients (e.g., Ref. [21]) to an extent to affect the meniscus dynamics substantially. Along with the assumption of adiabatic conditions, it was assumed that the gas phase was saturated with vapor of the liquid phase and that these phases were in thermal equilibrium. As a consequence, enthalpy changes and phase transitions were not included explicitly in either of the phases.

B. Effect of multiple miscible components

Fluids made of multiple miscible components may exhibit physical and chemical properties that are a function of their molar composition. For the gas phase, air is a typical example of nonideal gas, and its properties are well known [22]. For the liquid phase, the bulk physical and chemical mixture characteristics have been described making use of linear or nonlinear combinations of molar, volume, or mass fractions, as well as other thermodynamic parameters of the pure components.

A general linear binary mixing rule of the homologue parameters X_i and X_j of two components, i and j, allows determining the bulk parameter X of their mixture as

$$X=x_iX_i+x_jX_j, \tag{5}$$

with x_i and x_j the mass fractions of components i and j [23]. Equation (5) applies with relatively high accuracy to the viscosity μ_l of liquid mixtures of ideal and nonideal liquids and has been used on the same basis for the thermodynamic parameters n and K^0 governing the dynamic contact angle θ in Ref. [11]. Equation (5) can presumably be applied to the contact angle at rest θ_∞, but evidence of accuracy is not known yet. When the liquid components do not lead to reactions after coming into contact, Eq. (5) can be used also to determine the density ρ_l of liquid mixtures. When ρ_l is nonlinearly dependent on x_i and x_j, other approaches can be used that base on the virial equations for mixtures and are well described in Ref. [23] but were not used here as motivated later. Equation (5) may apply to the surface tension γ of inorganic compounds in aqueous solution, but it is known to depart from experiments for organic compounds [23]. In this case, γ can be described with an error less than 10% with the TKO approach (named after Ref. [24])

$$\gamma^{1/4}=\varphi_{s_w}\gamma_w^{1/4}+\varphi_{s_j}\gamma_j^{1/4}, \tag{6}$$

where φ_{s_w} and φ_{s_j} are the superficial volume fraction of water and component j, which can be determined by solving the following two equations:

$$\log\left(\frac{\varphi_{s_w}}{\varphi_{s_j}}\right)=\log\left(\frac{\varphi_w}{\varphi_j}\right)+\frac{0.441q}{T}\left(\frac{\gamma_jV_j^{\frac{2}{3}}}{q}-\gamma_wV_w^{\frac{2}{3}}\right), \tag{7a}$$

$$\varphi_{s_w}+\varphi_{s_j}=1, \tag{7b}$$

with $\varphi_w=x_wV_w/(x_wV_w+x_jV_j)$ and $\varphi_j=x_jV_j/(x_wV_w+x_jV_j)$, respectively, V_w and V_j the molar volumes of water and component j, q the number of carbon atoms in component j, and T the temperature.

Equations (5) and (6) allow therefore to determine ρ_l, μ_l, γ, n, and K^0 for combinations of multiple liquid substances to be used in Eqs. (1) in adiabatic conditions and particularly suited the set of experiments of water-ethanol mixtures, where ethanol is an organic compound. Note that Eqs. (6) and (7) explicitly includes the temperature T.

C. Effect of temperature in adiabatic conditions

Physical parameters susceptible to the temperature are the dynamic contact angle θ, the surface tension γ, the fluids densities (ρ_l and ρ_g), and the fluids viscosities (μ_l and μ_g).

Temperature affects $\theta(T)$ by means of two mechanisms affecting the contact angle at rest θ_∞ (e.g., squalane [25]) and the way molecular displacement at the solid-liquid interface occurs during meniscus movement, respectively. While the first effect was not included here, the latter was explicitly accounted for in $\theta(T)$ by means of the thermodynamic function $A(T)$ in Eq. (4).

Temperature-dependent surface tension, density, and viscosity of pure components can be expressed by means of empirical scaling laws that describe $\rho(T)$, $\gamma(T)$, and $\mu(T)$ as nonlinear functions of a number of empirical parameters [23]. To date, large databases are available that collect both experimental and regressed quantities for a large number of substances. Regardless of the method of determination (by measurement or fitting), the functions $\rho(T)$, $\gamma(T)$, and $\mu(T)$ at a specific temperature T for each component and in adiabatic conditions can be used to determine the homologue quantities for liquid mixtures using Eqs. (5) and (6) at that temperature. Specifically to this work, experimental values were used as detailed later.

In the absence of temperature gradients, Marangoni effects producing gradients in surface tension at the solid-liquid-gas contact line were neglected, while azeotropic effects leading to equilibrium liquid and vapor phases with differing compositions at different temperatures were not explicitly included in Eq. (6). Azeotropic effects may be highly nonlinear and may have effects on the surface tension that are not yet fully understood; in this framework, it was assumed that azeotropic partitioning of liquid and gas phase composition may have only secondary effects in adiabatic conditions, while important effects may arise in nonadiabatic conditions.

D. Dimensionless numbers

The dimensionless capillary number ($\mathrm{Ca} = \mu v/\gamma$; i.e., viscous vs tension forces) and the Bond number ($\mathrm{Bo} = \rho g \ell^2/\gamma$; i.e., body forces vs tension forces, with ℓ a characteristic length scale) can be used to determine which parameter controls the system state. For multiphase and multicomponent systems, Ca and Bo were to be adapted as time-, temperature-, and phase-dependent quantities as

$$\mathrm{Ca} = \frac{[h\mu_l + (L-h)\mu_g]h'}{L\gamma\cos(\theta)} = \frac{\mu(h)h'}{\gamma\cos(\theta)}, \tag{8}$$

$$\mathrm{Bo} = \frac{[h\rho_l + (L-h)\rho_g]gR^2}{L\gamma\cos\theta} = \frac{\rho(h)gR^2}{\gamma\cos(\theta)}. \tag{9}$$

E. Experiments with water-ethanol mixtures

The experimental equilibrium rise h_∞ of water-ethanol mixtures displacing air in a cylindrical Pyrex glass capillary for eight ethanol dilutions ranging from 0.023 to 0.9277 at temperatures between 20 and 86 °C were used from Ref. [26]. In these experiments, $L = 25$ cm was known, while $R = 0.3296$ mm was determined *a posteriori* (see details in Ref. [26]). The mixture density and temperature were measured and were combined with the readings of h_∞ to determine the temperature-dependent mixture surface tension.

Adiabatic conditions in the experiments were ensured by a thermal bath that maintained the capillary tube and the inner solution at a constant temperature. Temperature-induced density stratification within the bath was reduced by means of a mixer; this allowed to reduce (if not fully prevented) any temperature gradient inside the capillary. Hence, with the suitable time for the liquid and gaseous phase to reach equilibrium compositions, the experiments were run in the absence of latent heat effects, temperature gradients, and heat fluxes through the boundary.

For our analysis of this multiphase and multicomponent system, temperature-dependent $\rho(T)$, $\mu(T)$, and $\gamma(T)$ of air, water and ethanol were taken from chemical databases [27–29] and are represented in Fig. 1. The parameters $n = 4.58 \times 10^{20}$ m^{-2} and $K^0 = 4.038 \times 10^{10}$ s^{-1} for pure water, and $n = 1.442 \times 10^{16}$ m^{-2} and $K^0 = 251.85$ s^{-1} for pure ethanol, required for Eq. (4), were determined in Ref. [9] against experiments in Ref. [18]. These parameters were used in Eqs. (5) and (6) to determine those of water-ethanol mixtures.

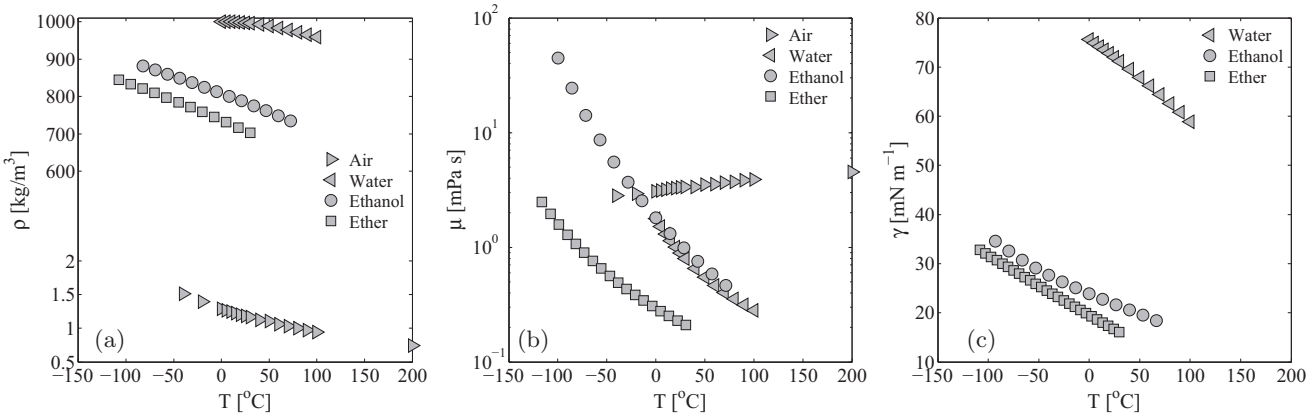

FIG. 1. Temperature-dependent density (ρ), viscosity (μ) and surface tension (γ) for air, water, ethanol (ethyl alcohol), and (diethyl) ether. Temperatures of liquids were limited between the melt and boil points at atmospheric pressure. Data sources: air [27]; water [28]; ethanol and ether [29].

TABLE I. Summary of experimental and modeled parameters (columns 3–4, and columns 6–10, respectively) for the air and water-ethanol mixtures as a function of ethanol mass fraction (column 1) and temperature (column 2). Columns 5 and 11 report the experimental and modeled equilibrium capillary height, respectively. Columns 12–14 report the relative percent error of modeled as compared to experimental parameters calculated as $(x - x_{\text{exp}})/x_{\text{exp}} \times 100$, with x the generic parameter.

		Experimental			Model						Residuals		
	2	3	4	5	6	7	8	9	10	11	12	13	14
1	T	ρ	γ	h_∞	ρ_l	ρ_g	μ_l	μ_g	γ	h_∞	$\Delta\rho$	$\Delta\gamma$	Δh_∞
f	(°C)	(kg/m^3)	(mN/m)	(mm)	(kg/m^3)	(kg/m^3)	(mPa s)	(μPa s)	(mN/m)	(mm)	(%)	(%)	(%)
0.0230	30.0	991.4	60.2	32.7	990.7	1.165	0.802	18.6	66.0	36.4	−0.1	9.7	11.2
	44.6	987.2	58.3	31.8	985.1	1.119	0.607	19.1	63.7	35.3	−0.2	9.3	11.0
	59.2	979.2	56.7	31.2	978.2	1.064	0.475	19.7	61.4	34.2	−0.1	8.2	9.7
	73.7	970.2	55.3	30.7	970.0	1.018	0.387	20.4	58.9	33.1	−0.0	6.5	7.9
	88.9	961.4	52.6	29.5	960.2	0.975	0.320	21.3	56.2	32.0	−0.1	6.9	8.3
0.0594	24.7	986.2	54.1	29.6	984.4	1.185	0.908	18.5	60.1	33.3	−0.2	11.0	12.5
	40.6	982.1	52.0	28.6	978.7	1.126	0.655	18.7	57.7	32.2	−0.4	11.1	12.6
	59.1	973.2	50.1	27.8	969.7	1.064	0.479	19.7	54.9	30.9	−0.4	9.6	11.2
	74.5	963.5	47.4	26.6	960.6	1.016	0.385	20.5	52.4	29.8	−0.3	10.6	12.0
0.1593	24.3	972.7	41.8	23.3	963.3	1.187	0.935	18.5	47.5	26.9	−1.0	13.6	15.5
	39.6	966.4	40.0	22.5	956.8	1.129	0.683	18.7	45.5	26.0	−1.0	13.8	15.4
	54.8	957.6	38.0	21.6	948.7	1.085	0.525	19.6	43.5	25.0	−0.9	14.5	15.9
	70.1	947.4	35.7	20.5	939.3	1.029	0.415	20.3	41.4	24.1	−0.9	16.0	17.4
	88.6	932.4	33.2	19.4	926.3	0.976	0.327	21.3	38.8	22.9	−0.7	16.8	17.8
0.2967	25.8	949.3	33.0	19.0	933.4	1.181	0.928	18.5	37.5	21.9	−1.7	13.5	15.3
	42.4	947.3	32.1	18.5	924.4	1.123	0.668	18.9	35.6	21.0	−2.4	10.9	13.6
	54.4	929.8	31.0	18.2	917.0	1.087	0.544	19.6	34.2	20.4	−1.4	10.4	11.9
	69.5	917.4	29.7	17.7	906.6	1.031	0.429	20.3	32.4	19.5	−1.2	9.2	10.3
	86.2	904.5	28.6	17.3	893.8	0.983	0.342	21.1	30.4	18.5	−1.2	6.2	7.2
0.4376	28.1	916.0	28.2	16.9	901.9	1.172	0.906	18.6	31.3	19.0	−1.5	11.1	12.2
	39.7	911.4	27.7	16.7	894.6	1.128	0.723	18.7	30.2	18.4	−1.8	8.9	10.2
	55.6	898.6	26.8	16.4	883.4	1.082	0.547	19.6	28.5	17.6	−1.7	6.4	7.4
	70.9	886.0	25.5	15.8	871.6	1.026	0.431	20.3	26.9	16.8	−1.6	5.5	6.6
	81.5	876.7	25.0	15.7	862.8	0.995	0.372	20.8	25.7	16.3	−1.6	2.9	3.7
0.6110	25.8	884.8	26.6	16.5	866.2	1.181	0.984	18.5	27.1	17.1	−2.1	1.8	3.4
	39.2	874.4	25.8	16.2	856.2	1.130	0.757	18.7	25.8	16.5	−2.1	0.1	1.7
	54.0	859.9	24.7	15.8	844.3	1.089	0.582	19.6	24.5	15.8	−1.8	−1.0	0.1
	69.7	843.7	23.8	15.5	830.8	1.030	0.452	20.3	22.9	15.1	−1.5	−3.6	−2.7
	81.3	834.6	22.6	14.9	820.1	0.996	0.382	20.8	21.8	14.5	−1.7	−3.6	−2.7
0.7568	20.1	851.9	25.4	16.4	839.7	1.204	1.141	18.2	25.1	16.3	−1.4	−1.3	−0.7
	26.8	848.4	25.0	16.2	834.2	1.177	0.988	18.5	24.5	16.0	−1.7	−2.1	−1.2
	40.4	834.5	23.8	15.7	822.7	1.126	0.760	18.7	23.3	15.5	−1.4	−2.2	−1.6
	51.7	824.6	22.6	15.1	812.6	1.101	0.623	19.5	22.3	15.0	−1.5	−1.3	−0.8
	62.7	812.5	21.8	14.8	802.4	1.052	0.518	19.9	21.3	14.5	−1.2	−2.2	−2.0
	72.5	804.7	21.3	14.6	793.0	1.022	0.443	20.4	20.4	14.1	−1.5	−4.1	−3.7
	81.2	797.0	20.5	14.2	784.2	0.996	0.390	20.8	19.6	13.6	−1.6	−4.4	−3.9
0.9272	25.5	806.4	22.9	15.6	798.9	1.182	1.047	18.5	22.5	15.4	−0.9	−1.9	−1.6
	38.5	796.6	22.0	15.2	786.4	1.133	0.815	18.7	21.4	14.9	−1.3	−2.7	−2.3
	49.2	782.4	21.0	14.8	775.8	1.110	0.672	19.4	20.5	14.4	−0.8	−2.3	−2.4
	58.5	775.9	20.4	14.8	766.4	1.067	0.569	19.7	19.7	14.1	−1.2	−3.2	−5.0
	69.0	765.3	19.7	14.2	755.4	1.032	0.481	20.2	18.8	13.6	−1.3	−4.3	−4.1
	78.7	756.3	19.2	14.0	744.9	1.003	0.415	20.6	18.0	13.2	−1.5	−6.2	−5.8

F. Experiments with ether

Experimental dynamic rise of pure (diethyl) ether displacing air was used from Ref. [16]. The experiments were carried out using a cylindrical glass capillary with radius $R = 0.689$ mm; the length L was not reported in Ref. [16], but it was assumed to be $L = 10$ cm. Temperature-dependent values of $\rho(T)$, $\mu(T)$, and $\gamma(T)$ for air were from Blevins [27] and for ether were from Ref. [29] (Fig. 1). For these multiphase and single-component systems, the mixing rules were not used.

Conversely to water-ethanol experiments, we have no evidence that a specific system was designed to reduce heat exchange and minimize temperature gradients in the experiments in Ref. [16]. We assumed that experimental good practice was such that an equilibrium temperature was reached at the time readings were taken and that (near) adiabatic conditions were achieved also in this case.

The data in Ref. [16] were particularly interesting because they showed oscillations around the equilibrium rise h_∞ and could be used to investigate effects of temperature on those oscillations.

G. Numerical solution of the governing equation

The second-order problem in h'' of Eq. (1) was solved by decomposing it into two first-order differential equations, which were numerically integrated with a direct explicit finite-difference technique. Note that no parameter estimation was carried out against experimental values.

III. RESULTS

Our study of temperature-dependent capillary dynamics is divided in two analyses: one focused on water-ethanol mixtures, and one focused on ether. Results are presented here in tabular and graphical form.

A. Temperature-dependent rise of water-ethanol mixtures

The experimental data described in Section 2.6 from Ref. [26] were used with the temperature- and water-ethanol mixture-dependent capillary rise of Eq. (1).

Table I summarizes the experimental parameters at various ethanol mass fractions f and temperatures T, for comparison with those calculated using Eqs. (5) and (6), and the corresponding experimental and modeled equilibrium rise h_∞, the latter determined as

$$h_\infty = \frac{2\gamma(f,T)\cos(\theta_\infty)}{\rho_l(f,T)Rg},$$

with the contact angle at rest $\theta_\infty = 0$ as per data in Ref. [18].

Here we note that an increasing f (column 1 in Table I) resulted in a decreasing h_∞ (column 5 in Table I). This aspect was explained by γ for ethanol being sensibly lower than that of water. We also note that higher T (column 2) resulted in an additional lowering in h_∞, which was not negligible. In fact, γ decreases at higher T for both water and ethanol [Fig. 1(c)], and hence also for the water-ethanol mixtures.

The parameters calculated by the mixing rules in Eqs. (5) and (6) are listed in columns 6–10 of Table I. Here we note that a linear mixing rule applied to the mixture density generally underestimated the experimental density. However, we note that underestimation was small as the relative percent error (residual) ranged between less than 0.01% to 2.4% (column 12). The calculated values of the surface tension using the nonlinear mixing rule of Eq. (6) led to residuals ranging between 0.1% to 13%, with an average of 6.9%.

When the parameters calculated by the mixing rules were used in Eq. (1) (Columns 6–10, Table I), h_∞ departed from experiments by a maximum of about 15% for ethanol fractions $f = 0.1593$ and 0.2967 (column 14, Table I). The relative percent error was lower in all other tests.

We identified three sources of uncertainty to the exact calculation of h_∞. The error in estimating h_∞ was due to the mixture density $\rho_l(f,T)$ to a minor extent and to the surface tension $\gamma(f,T)$ to a larger extent, which was generally higher than experimental ones for $f < 0.6$ and lower for $f > 0.6$. An unmeasurable contribution to the errors came from the method of experimental determination of γ and R, which were calculated by inverse problem solving in Ref. [26] and did not include possible temperature effects in θ_∞. Accordingly, θ_∞ was assumed here not to change with T.

Simulations of the capillary rise over time calculated with Eq. (1) are shown in Fig. 2(a) only for the experimental ethanol mass fraction $f = 0.611$, where a monotonic rise was observed. We remark that monotonic rise without oscillations of the meniscus was found in all cases of Table I. It is important though to comment that, for some values of R, higher or lower T may result in transitions in $h(t)$ from monotonic to oscillatory around h_∞. To show this behavior, a simulation was run for $f = 0.611$ but with $R = 2$ mm and for T ranging between -50 and 80 °C, i.e., within melt (lower than -50 °C) and boil (82 °C) temperatures of that water-ethanol mixture. This range of temperatures does not include the azeotropic point (minimum mixture boiling temperature) and implies that the liquid and gaseous equilibrium compositions at various temperatures were different [30]. These different compositions may have an effect on the surface tension in addition to those related to the temperature T, mixture composition f, and

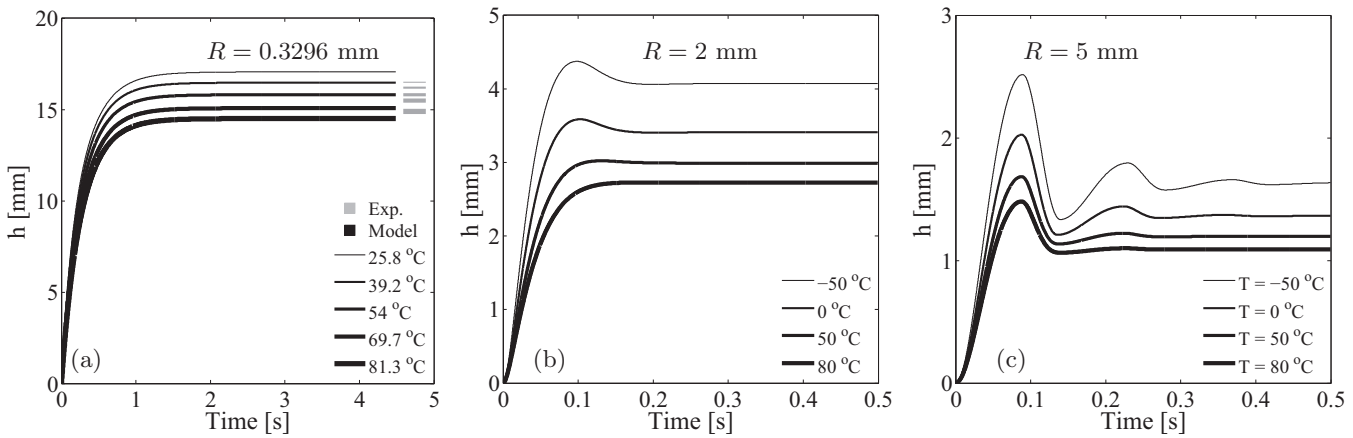

FIG. 2. Experimental and modeled rise of a water-ethanol mixture displacing air in a glass capillary. The ethanol mass fraction $f = 0.611$ was used at various temperatures for rise in capillaries with radius (a) $R = 0.3296$ mm, (b) $R = 2$ mm, and (c) $R = 5$ mm. Experimental data in (a) are from Ref. [26].

carbon atoms content q in ethanol already included in Eq. (6), but these effects may be of higher order. Figure 2(b) shows that a one-bounce oscillation for $T < 80\,^{\circ}$C had an oscillation amplitude and equilibrium rise h_∞ decreasing as T increased until the rise became monotonic at $T = 80\,^{\circ}$C. The same test was repeated for $R = 5$ mm, and the results in Fig. 2(c) show multiple oscillations at lower T. This transition was related to the specific balance among weight, viscous, and surface forces acting on the liquid and gaseous phases and is investigated in greater detail later.

It is interesting to note in Fig. 2(c) that the velocity h' was not uniform over time and was not symmetric with respect to the flow direction. In fact, Eq. (1) is asymmetric with the flow direction because dissipations depended on whether jet flow (capillary outlet) and reservoir retardation (capillary inlet) occurred in the gas and liquid phase, respectively, or vice versa. Faster rise and slower receding velocities [Fig. 2(c)] were largely determined by the length of capillary occupied by the gas phase, and by viscous dissipation more important in the liquid reservoir during recession than in the gaseous reservoir during rise. These effects are not commonly accounted for in the existing formulations of the LW equation, with the exception of the work in Ref. [31] for the liquid phase. Here, however, asymmetric energy dissipation was included in Eq. (1) for both liquid and gaseous phases and allowed us to evidence its effects.

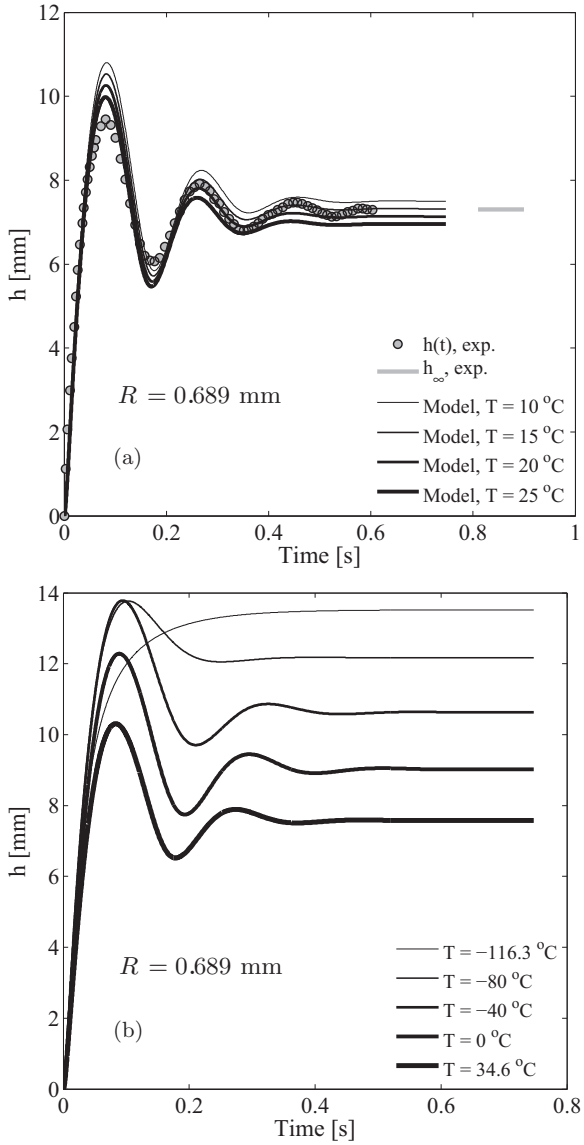

FIG. 3. (a) Experimental and modeled rise over time of ether displacing air in a glass capillary of radius $R = 0.689$ mm. Experimental data are redrawn from [16]. (b) Temperature sensitivity of rise for the same system as in (a).

B. Temperature-dependent rise of ether

Experiments of ether rise described in Section 2.7 from Ref. [16] were used in our analysis of temperature-dependent capillary rise.

The experimental capillary rise at rest $h_\infty = 7.3$ mm, and the values $\gamma = 16.6$ mN m^{-1} and $\rho_l = 710$ kg m^{-3} for ether in the original work suggested that the contact angle was very small, hence $\theta_\infty = 0$ was assumed to solve Eq. (1). Values of

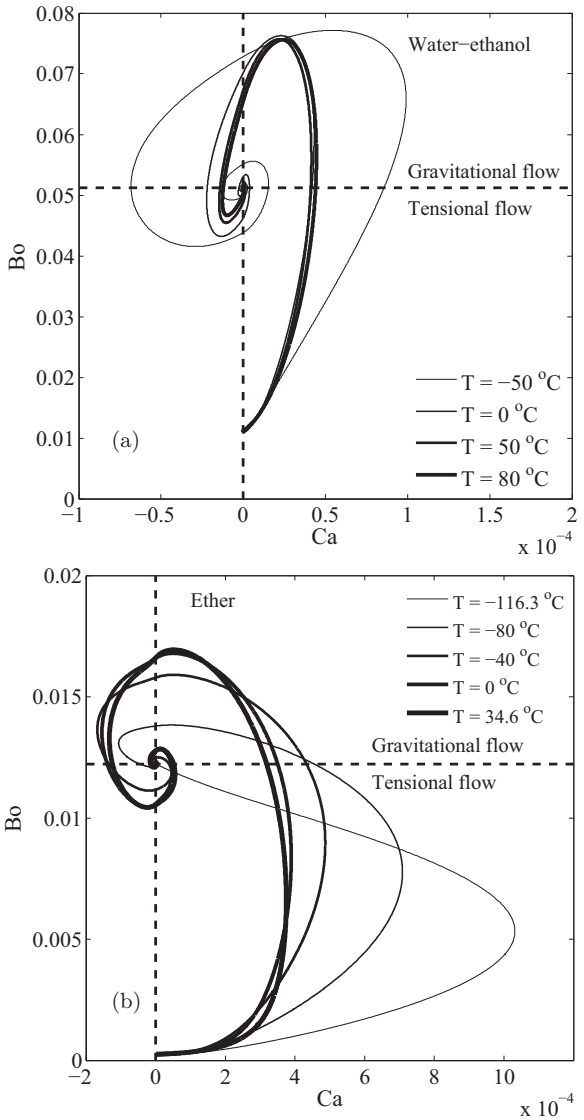

FIG. 4. Temperature sensitivity of Ca-Bo orbits for (a) water-ethanol rise ($f = 0.611$) from Fig. 2(c), and for (b) ether rise from Fig. 3(b).

$\rho_l(T)$ and $\rho_g(T)$, $\mu_l(T)$ and $\rho_g(T)$, and $\gamma(T)$ for air and ether were used as per Fig. 1. Temperatures ranging from 10 to 25 °C, tested for comparison with experimental data, showed to be relatively accurate in capturing the experimental capillary height $h(t)$ over time, the oscillation frequency, and the damping rate with an error smaller than 15% in the first oscillation at about 0.1 s (Fig. 3). A temperature comprised between 15 and 20 °C returned the observed h_∞ and was remarkably realistic for laboratory conditions (unfortunately the experimental temperature was not reported in the original work).

A series of simulations for ether rise was run with temperatures ranging from melt (−116.3 °C) to boil (34.6 °C) points to highlight transitions in the dynamical approach to h_∞. Figure 3(b) shows also in this case that temperature expressed a role in determining the characteristics of multiphase flows in capillaries. T increments induced a visible transition from nonoscillatory ($T = -116.3$ °C) to oscillatory ($T \geqslant -80$ °C). This transition was caused by a changing balance between body, viscous, and surface forces. Higher temperatures resulted also in a lower equilibrium rise h_∞, a lower damping, and a higher oscillation frequency in the oscillatory regime.

C. Ca-Bo orbits of temperature-dependent rise

A careful inspection of Fig. 2(b) and 2(c) for ethanol-water rise and Fig. 3(b) for ether rise highlights an important feature in the way how temperature affects oscillations. In fact, higher T lowered the oscillation amplitude for water-ethanol mixtures and increased that of ether. These dynamics can be better represented in the dimensionless space Ca-Bo with the dimensionless numbers Ca and Bo as in Eqs. (8) and (9).

The Ca-Bo orbits (continuous lines in Fig. 4) showed a characteristic "ear" shape and converged to a fix-point attractor when $h \to h_\infty$. The dashed lines indicate the values of Ca and Bo at rest and split the space in regions characterized by different regimes of flow. Among them, the gravitational and tensional flow regimes delimited by Bo at rest are the most important for oscillations, while Ca $\neq 0$ occurred when $h' \neq 0$ led to viscous dissipation.

Water-ethanol rise was dominated by gravitational flow for all temperatures tested here as all orbits reached about the same maximum value Bo $\simeq 0.075$ [Fig. 4(a)]. However, higher temperatures resulted in a decreased h' and lower values of |Ca|. On the other hand, the Ca-Bo orbits of ether rise appeared to be dominated by tensional flow at low temperature (Bo did not exceed the equilibrium values), but any increase in T resulted in progressively increasing values of Bo, with the orbits becoming narrower on the Ca direction and elongated along the Bo direction [Fig. 4(b)]. An increase in T caused a decreased viscous dissipation as in the water-ethanol Ca-Bo orbits, but showed that tension at the solid-liquid-gas interface in this system was the dominant temperature-dependent driver of rise.

IV. CONCLUDING REMARKS

A generalized formalism for multiphase and multicomponent flows in capillary tubes was used to explicitly analyze the effect of temperature on the meniscus dynamics approaching equilibrium in adiabatic conditions. The mathematical framework, tested on experiments of various ethanol-water mixtures and ether rise in uniform cylindrical capillaries, demonstrated that the temperature can largely influence the dynamics of flow around the attractor. In particular, temperature dictates transition to the oscillatory regime. These characteristics can be predicted relatively accurately as long as the scaling relationship between physical parameters and temperature are mechanistically or empirically known. Evidence is such that comparison with experiments led to residuals not exceeding 15%, with an average of about 7% in most cases, and with no need to estimate parameters.

ACKNOWLEDGMENTS

We thank the two anonymous reviewers for their contribution in making the manuscript clearer, especially in that concerned with the azeotropic effects in capillary dynamics. We thank also Celia Lozano for her help with editing the original manuscript.

[1] J. M. Bell and F. K. Cameron, J. Phys. Chem. **10**, 658 (1906).
[2] R. Lucas, Colloid Polym. Sci. **23**, 15 (1918).
[3] E. W. Washburn, Phys. Rev. **17**, 273 (1921).
[4] T. D. Blake and J. M. Haynes, J. Colloid Interface Sci. **30**, 421 (1969).
[5] J. Szekely, A. W. Neumann, and Y. K. Chuang, J. Colloid Interface Sci. **35**, 273 (1971).
[6] S. Levine, J. Lowndes, E. J. Watson, and G. Neale, J. Colloid Interface Sci. **73**, 136 (1980).
[7] M. Dreyer, A. Delgado, and H.-J. Path, J. Colloid Interface Sci. **163**, 158 (1994).
[8] B. V. Zhmud, F. Tiberg, and K. Hallstensson, J. Colloid Interface Sci. **228**, 263 (2000).
[9] F. Maggi and F. Alonso-Marroquin, Int. J. Multiphase Flow **42**, 62 (2012).
[10] S. Das and S. K. Mitra, Phys. Rev. E **87**, 063005 (2013).
[11] F. Maggi, Colloids Surf. A **415**, 119 (2012).
[12] M. C. Phillips and A. C. Riddiford, Nature **205**, 1005 (1965).
[13] A. V. Kuźmich and V. I. Novikova, J. Eng. Phys. Thermophys. **57**, 1298 (1989) [Translated from Inzhenerno-Fizicheskii Zhurnal **57**(5), 750 (1989), by S. M. Kirov].
[14] P.-G. De Gennes, Rev. Mod. Phys. **57**, 827 (1985).
[15] S. Sugden, J. Chem. Soc. Trans. **125**, 1177 (1924).
[16] D. Quéré, É. Raphaël, and J.-Y. Ollitrault, Langmuir **15**, 3679 (1999).
[17] D. Quéré, Europhys. Lett. **39**, 533 (1997).
[18] A. Hamraoui, K. Thuresson, T. Nylander, and V. Yaminsky, J. Colloid Interface Sci. **226**, 199 (2000).
[19] M. Stange, M. E. Dreyer, and H. J. Rath, Phys. Fluids **15**, 2587 (2003).
[20] G. Martic, F. Gentner, D. Seveno, D. Coulon, J. De Coninck, and T. D. Blake, Langmuir **18**, 7971 (2002).
[21] K. Nagai, Y. Sumino, H. Kitahata, and K. Yoshikawa, Phys. Rev. E **71**, 065301 (2005).

[22] D. A. Chin, A. Mazumdar, and P. K. Roy, *Water-Resources Engineering*, 2nd ed. (Pearson Education Inc., Upper Saddle River, NJ, 2000), p. 962.
[23] R. C. Reid and T. K. Sherwood, *The Properties of Gases and Liquids*, 2nd ed. (McGraw-Hill, New York, 1966), p. 646.
[24] M. Tamura, M. Kurata, and H. Odani, Bull. Chem. Soc. Jpn. **28**, 83 (1955).
[25] M. De Ruijter, P. Kölsch, M. Voué, J. De Coninck, and J. P. Rabe, Colloid Surface A **144**, 235 (1998).
[26] W. S. Bonnell, L. Byman, and D. B. Keyes, Ind. Eng. Chem. **32**, 532 (1940).
[27] R. D. Blevins, *Applied Fluid Dynamics Handbook* (Van Nostrand Reinhold, New York, 1984), p. 568.
[28] E. Finnemore and J. B. Franzini, *Fluid Mechanics with Engineering applications*, 10th ed. (McGraw-Hill, Inc., New York, NY, 2002), p. 816.
[29] J. Gmehling and C. Möllmann, Ind. Eng. Chem. Res. **37**, 3112 (1998).
[30] A. I. Vogel, *Practical Organic Chemistry*, 3rd ed. (Longman group limited, London, 1974), p. 1188.
[31] É. Lorenceau, D. Quéré, J.-Y. Ollitrault, and C. Clanet, Phys. Fluids **14**, 1985 (2002).